Atmospheric Environment 45 (2011) 7151–7165

Contents lists available at SciVerse ScienceDirect

Atmospheric Environment

journal homepage: www.elsevier.com/locate/atmosenv

Multi-spectral sensitivity studies for the retrieval of tropospheric and lowermost tropospheric ozone from simulated clear-sky GEO-CAPE measurements

Vijay Natraj[a,*], Xiong Liu[b], Susan Kulawik[a], Kelly Chance[b], Robert Chatfield[c], David P. Edwards[d], Annmarie Eldering[a], Gene Francis[d], Thomas Kurosu[a], Kenneth Pickering[e], Robert Spurr[f], Helen Worden[d]

[a] Jet Propulsion Laboratory, California Institute of Technology, 4800 Oak Grove Drive, Pasadena, CA 91109, USA
[b] Harvard-Smithsonian Center for Astrophysics, 60 Garden Street, Cambridge, MA 02138, USA
[c] NASA Ames Research Center, Moffett Field, CA 94035, USA
[d] National Center for Atmospheric Research, PO Box 3000, Boulder, CO 80307, USA
[e] NASA Goddard Space Flight Center, Greenbelt, MD 20771, USA
[f] RT Solutions, Inc., 9 Channing Street, Cambridge, MA 02138, USA

ARTICLE INFO

Article history:
Received 7 February 2011
Received in revised form
7 September 2011
Accepted 7 September 2011

Keywords:
Multi-spectral
Ozone
Retrieval
Sensitivity
Troposphere
Geostationary platform
GEO-CAPE

ABSTRACT

One of the important science requirements of the Geostationary Coastal and Air Pollution Events (GEO-CAPE) mission is to be able to measure ozone with two degrees of freedom in the troposphere and sensitivity in the lowest 2 km (lowermost troposphere, LMT), in order to characterize air quality and boundary layer transport of pollution. Currently available remote sensing techniques utilize backscattered solar ultraviolet (UV) radiances or thermal infrared (TIR) emissions to perform ozone retrievals. However, in the TIR, measurement sensitivity to the LMT requires high thermal contrast between the Earth's surface and the near-surface (tens to hundreds of meters above surface) atmosphere, while in the UV, the measurement sensitivity to the LMT is low because of Rayleigh scattering. In this paper, we explore the feasibility of using multi-spectral intensity measurements in the UV, visible (VIS), mid infrared (MIR) and TIR, and polarization measurements in the UV/VIS, to improve tropospheric and lowermost tropospheric ozone retrievals.

Simulations for 16 cloud and aerosol free atmospheric profiles spanning a range of ozone mixing ratios indicate that adding VIS measurements to UV measurements significantly enhances the sensitivity to lowermost tropospheric ozone, but only makes a slight improvement to the total degrees of freedom for signal (DFS). On the other hand, the combination of UV and TIR significantly improves the total DFS as well as the lowermost tropospheric DFS.

The analysis presented here is a necessary and important first step for defining spectral regions that can meet the GEO-CAPE measurement requirements, and subsequently, the requirements for instrumentation. In this work, the principle of multi-spectral retrievals has been extended from previously published literature and we show that the UV + VIS, UV + TIR and UV + VIS + TIR combinations have the potential to meet the GEO-CAPE measurement requirements for tropospheric ozone. Our analysis includes errors from water and surface properties; further analysis is needed to include temperature, additional gas interferents, clouds, aerosols and more realistic surface properties. These simulations must be run on a much larger dataset, followed by OSSEs (Observing System Simulation Experiments), where simulated retrievals are assimilated into chemical-transport models, to quantitatively assess the impact of the proposed measurements for constraining the spatiotemporal distribution of ozone in the LMT for basic science studies and applications such as air quality forecasts.

1. Introduction

1.1. Ozone, air quality and the GEO-CAPE mission

Ozone is one of the key regulated air pollutants (see, e.g., Akimoto, 2003), yet our current observation system is severely limited in the spatial coverage of time-resolved measurements. Ozone is a secondary pollutant, and its formation is non-linear and

* Corresponding author. Tel.: +1 818 354 9229; fax: +1 818 354 5148.
E-mail address: Vijay.Natraj@jpl.nasa.gov (V. Natraj).

1352-2310/$ – see front matter © 2011 Elsevier Ltd. All rights reserved.
doi:10.1016/j.atmosenv.2011.09.014

dependent on primary precursor emissions, transport, and atmospheric chemistry, where it plays a major role in determining the atmospheric oxidizing capacity (see, e.g., Seinfeld and Pandis, 2006). In the lowermost troposphere (LMT), defined here as the lowest 2 km, ozone is toxic to humans and crops (see, e.g., Boubel et al., 1994). Throughout the troposphere, ozone is also a very important greenhouse gas (IPCC, 2007). For the effective prediction of air pollution and the development of control strategies, the high spatial and temporal variability of ozone and other pollutants must be better quantified (see, e.g., Martin, 2008).

Using input from the broad Earth science community, the National Research Council (NRC) developed a comprehensive blueprint for the development and implementation of the next generation of Earth science satellite missions (NRC, 2007). The Geostationary Coastal and Air Pollution Events (GEO-CAPE) mission was recommended for launch in an intermediate timeframe. One of the four major objectives of the GEO-CAPE mission as defined by the Decadal Survey (NRC, 2007) is to provide the research and operational air quality communities with information on the natural and anthropogenic emissions of ozone and aerosol precursors. The GEO-CAPE science working group has specified the need to measure ozone with two degrees of freedom (pieces of information) in the troposphere and sensitivity in the LMT, in order to characterize air quality and boundary layer transport of pollution. Because of its importance in so many aspects of atmospheric chemistry, an accurate measurement of ozone with the maximum possible vertical resolution in the troposphere is a fundamental aspect in the design of the instruments that will make up GEO-CAPE. The science working group has developed a Science Traceability Matrix giving mission threshold and baseline requirements for measurements of tropospheric ozone and other pollutant and diagnostic gases, such as NO_2, CO, HCHO, CHOCHO, CH_4, SO_2, and NH_3, as well as aerosol properties. Similar missions for monitoring air quality from geostationary platforms have been proposed for Europe (see, e.g., Burrows et al., 2004; Langen, 2007; Stuhlmann et al., 2005), Japan (see, e.g., Akimoto et al., 2008, 2009) and Korea (see, e.g., Kim et al., 2009; Lee et al., 2010). A full summary of the geostationary air quality missions planned for launch in the 2017–2020 timeframe is reported in a recent Committee on Earth Observation Satellites (CEOS) document (CEOS, 2011).

1.2. Current capabilities for measuring tropospheric ozone from space

At present, tropospheric ozone profiles are measured from instruments on Low Earth Orbiting (LEO) satellites, using backscattered ultraviolet (UV) radiation, such as the Global Ozone Monitoring Experiment (GOME) (Liu et al., 2005, 2006) and the Ozone Monitoring Instrument (OMI) (Liu et al., 2010a,b), or thermal infrared (TIR) radiation, such as the Tropospheric Emission Spectrometer (TES) (Beer, 2006), the Infrared Atmospheric Sounding Interferometer (IASI) (Boynard et al., 2009; Clerbaux et al., 2009; Dufour et al., 2010; Eremenko et al., 2008), and the Atmospheric Infrared Sounder (AIRS) (Aumann et al., 2003). The Microwave Limb Sounder (MLS) provides ozone profiles for the upper troposphere and stratosphere that can be combined with OMI data to derive a tropospheric ozone column (see, e.g., Ziemke et al., 2006). Vertical sensitivity is limited for UV-only or TIR-only instruments. For example, OMI ozone retrievals demonstrate ~1 degree of freedom for signal (DFS) in the troposphere with ~10 km vertical resolution (Liu et al., 2010b) and TES ozone retrievals have ~1.5 DFS in the troposphere with 6–7 km vertical resolution (Jourdain et al., 2007). The degrees of freedom for signal are a measure of the number of useful independent pieces of information available from the measurements (Rodgers, 2000). While LEO satellite instruments provide global measurements, they only sample once per day during daylight, which gives little insight into ozone evolution over the diurnal cycle. However, an instrument in geostationary orbit would provide the temporal resolution (~1 h) needed to observe the short-term variability in emissions, photochemistry, mixing, and transport that is critical for characterizing air quality. Ultimately, both Geostationary Earth Orbit (GEO) and LEO measurements are necessary to fully understand the components of global composition change (CEOS, 2011). Observations from a single LEO satellite would overlap those from each GEO satellite once per day (twice per day if we include measurements at night), providing a means for combining the GEO and LEO observations and a necessary perspective for interpreting the global impact of the smaller scale processes.

1.3. Multi-spectral retrieval approaches

The ability to retrieve ozone concentrations in the LMT is a requirement of the GEO-CAPE mission. A measure of lowermost tropospheric concentration in conjunction with the free tropospheric profile also allows local pollution production to be separated from transported pollution. Measurements in different parts of the electromagnetic spectrum have different sensitivities to the gas vertical distribution. In the TIR, measurement sensitivity to the LMT requires high thermal contrast between the Earth's surface and the near-surface (tens to hundreds of meters above surface) atmosphere. However, TIR measurements will always provide information in the free troposphere in cloud-free conditions. Measurements of reflected solar radiation in the mid infrared (MIR) and visible (VIS) parts of the spectrum are usually thought to contain total column information from the weak spectral features of interest. At the short wavelengths of the UV, measurement sensitivity to the LMT is low because of Rayleigh backscatter of the incoming solar radiation as the air density increases in the lower troposphere.

The benefits of a multi-spectral retrieval approach have been previously demonstrated for the UV and TIR combination using simulated radiances (Landgraf and Hasekamp, 2007; Worden et al., 2007). Adding polarization sensitivity to the UV retrieval should further increase the information content of joint retrievals (see, e.g., Hasekamp and Landgraf, 2002; Hasekamp et al., 2002; Jiang et al., 2004). In this paper, we explore the benefit of combining measurements in different spectral regions from the UV to the TIR to optimize ozone profile retrievals, with particular emphasis on the LMT. This work provides the information needed for Observing System Simulation Experiments (OSSEs) (see, e.g., Atlas, 1997; Claeyman et al., 2011; Edwards et al., 2009; Masutani et al., 2010; Timmermans et al., 2009), where simulated retrievals are assimilated (see, e.g., Kalnay, 2003) into chemical-transport models, to assess the impact of the proposed measurements on constraining the distribution of ozone in the LMT and the resulting benefits for applications such as air quality forecasts.

1.4. Outline

In Section 2, we outline the rationale for choosing specific spectral regions, and the corresponding spectral resolution, sampling interval and signal to noise ratio (SNR). In Section 3, we describe the scenarios used in the simulations. Sections 4 and 5 provide brief descriptions of the radiative transfer (RT) and inverse models, respectively. In Section 6, we present DFS and profile retrieval results for individual spectral regions and combinations. In Section 7, we discuss issues that might affect the results, including spectral resolution, sampling interval and SNR, surface polarization, spectroscopy and calibration consistency, and aerosols and clouds. We arrive at some preliminary conclusions in Section 8.

2. Spectral descriptions

2.1. Spectral ranges

The UV and VIS regions selected for this work are based on experience with previous instruments, specifically, SCIAMACHY (Bovensmann et al., 1999), the GOME instruments (Burrows et al., 1993; Chance et al., 1991, 1997; European Space Agency, 1995), and OMI (Levelt et al., 2006; OMI Algorithm Theoretical Basis Document, 2002). Tropospheric ozone measurements in the UV have concentrated on the spectral region 290–340 nm, as demonstrated in practical retrievals (Liu et al., 2005, 2010a,b). The VIS retrieval range discussed here (560–620 nm) has not yet been demonstrated for use in nadir retrievals, but is selected to include the most prominent structure in the Chappuis band (see, e.g., Brion et al., 1998). The TIR spectral region (980–1070 cm^{-1}) is based on ozone retrievals from the TES instrument (Bowman et al., 2002; Worden et al., 2004). The MIR spectral region (2780–2833 cm^{-1} and 3035–3055 cm^{-1}) is based on ozone retrievals using the Tropospheric Infrared Mapping Spectrometers (TIMS) prototype instrument (Kumer et al., 2009).

Cross sections for the UV and VIS regions are taken from the work of Daumont et al. (1992), Brion et al. (1993, 1998) and Malicet et al. (1995). The MIR and TIR cross sections are calculated from line parameters in HITRAN2008 (Rothman et al., 2009). Cross sections are calculated as Voigt line profiles using the pressures and temperatures of the respective atmospheric layers. We did not include the effects of inconsistent spectroscopy in the analysis for this paper. As long as the synthetic spectra and the reference data used in retrievals are self-consistent, such effects cancel in our study. For actual implementation, it will be necessary to improve the consistency among the various absorption and emission bands.

2.2. SNR, spectral resolution and sampling interval

The retrieval sensitivity to ozone from various spectral regions depends on the uncertainty, spectral resolution and spectral sampling of the measurements. These parameters as well as the spectral coverage are in turn critical for instrument design. The assumptions for these parameters are based on existing satellite or ground-based instruments. For this theoretical study, we only consider random-noise measurement error assuming that systematic errors can eventually be accounted for. This is a first step toward understanding multi-spectral retrievals in the LMT.

The SNR for the UV and VIS spectral regions is set using OMI observations. The SNR is calculated for each frequency using the formula:

$$\mathrm{SNR} = \mathrm{SNR}_{\mathrm{OMI}} \times 3 = \mathrm{sqrt}(R \times F_{\mathrm{sol}} \times \Delta\lambda/\Delta\lambda_0) \times 1250 \times 3 \quad (1)$$

where R is the normalized radiance, F_{sol} is the normalized solar irradiance at OMI resolution (with a value of 16 at 340 nm), $\Delta\lambda$ is the sampling interval in nm, and $\Delta\lambda_0$ is the average sampling interval (0.15 nm) in the OMI UV2 channel. The OMI SNR ($\mathrm{SNR}_{\mathrm{OMI}}$) is based on the fact that for a normalized radiance of 0.0625 at 340 nm (typical tropical clear-sky conditions at nadir), the SNR is ~1250. The multiplication by 3 is to reflect the technical capability of a UV/VIS instrument, which has already been achieved by GOME. The working assumption here is that a geostationary orbiting instrument could be built today with the SNR characteristics of a LEO instrument built 20 years ago. This formula implies a Noise Equivalent Source Radiance (NESR) of 3.645×10^9 photons/cm^2/s/nm/sr for the entire spectral region.

The NESR for the TIR spectral region is set using the TES instrument characteristics. One day's worth of TES global data was used to derive a simple relationship between the NESR and the radiance brightness temperature using the window region from 984 to 986 cm^{-1} (BT985). When BT985 is greater than 260 K, the relationship was found to be:

$$\mathrm{NESR} = 6.950 \times 10^{-9} + 5.133 \times 10^{-11} \times \mathrm{BT985} \quad (2a)$$

whereas if BT985 is less than 260 K, the best fit relationship was:

$$\mathrm{NESR} = -2.262 \times 10^{-9} + 8.663 \times 10^{-11} \times \mathrm{BT985} \quad (2b)$$

The NESR is then divided by 3 to represent the performance of the TES instrument if the electrical filters had functioned as originally planned. The NESR for a Fourier Transform Spectrometer like TES does not vary significantly with frequency (see, e.g., Worden et al., 2006). For this study the NESR was set to a constant value over the entire band.

The SNR for the MIR region is based on TIMS demonstration measurements, and assumes a 2 s integration time with a 8 km × 8 km footprint from geostationary orbit. The NESR was additionally divided by 3 from the calculated value, which could correspond to a larger footprint or a longer integration time or possible further improvement in instrumentation. Again, the NESRs scale with the observed mean frequency; for the cases we studied, the mean radiance for the 3035–3055 cm^{-1} (3.3 μm) region was 5.1×10^{-8} W cm^{-2} sr^{-1} $(cm^{-1})^{-1}$, and the mean NESR was 1.4×10^{-10} W cm^{-2} sr^{-1} $(cm^{-1})^{-1}$. For the 2780–2833 cm^{-1} (3.6 μm) region, the mean radiance was 6.6×10^{-9} W cm^{-2} sr^{-1} $(cm^{-1})^{-1}$ with a mean NESR of 7.1×10^{-11} W cm^{-2} sr^{-1} $(cm^{-1})^{-1}$.

The spectral resolution, used here to refer to the full-width at half-maximum (FWHM) of the slit function, in the UV is determined primarily by the needs for fitting of trace gases, including SO_2, BrO, HCHO, NO_2, and CHOCHO. The resolution needs for O_3 profile/tropospheric O_3 determination are not normally an instrument driver in the UV/VIS. Resolution needs for GEO-CAPE continue to be studied. The FWHM of the slit function will likely be on the order of 0.4 nm in the UV/VIS. In the TIR, we use the spectral resolution of TES, which was chosen to be on the order of 0.1 cm^{-1} to differentiate between stratospheric and tropospheric ozone based on pressure broadening (Beer, 1992). The resolving power of a grating instrument remains constant; measurements made in field intercomparisons (Kumer et al., 2008) demonstrate a spectral resolution of 0.18 cm^{-1} in the MIR.

Sampling requirements are determined by the need to limit distortion of measured spectra to a level that can be corrected by independent knowledge of the solar spectrum (Chance et al., 2005). For ozone measurements, this will be quite modest, perhaps as few as 2.5 spectral samples per slit FWHM.

For simplicity, we assume Gaussian slit functions for the instrument line shape (ILS). The ILSs are set to be similar to the above mentioned instruments, with FWHM values of 0.4 nm, 0.1 cm^{-1} and 0.18 cm^{-1} for the UV/VIS, TIR and MIR regions respectively. These slit functions are used in the convolution of the "monochromatic" radiances and weighting functions (Jacobians) that are calculated at very fine spectral resolution. The convolution produces the "observed" spectra and Jacobians; sampling is done at spectral intervals of 0.1 nm, 0.06 cm^{-1} and 0.02775 cm^{-1} in the UV/VIS, TIR and MIR regions respectively. The characteristics of the various spectral regions are summarized in Table 1.

The NESRs are set assuming the above spectral sampling. If a different spectral sampling is selected, the NESR must be adjusted by multiplying by $\sqrt{\text{current sampling}/\text{new sampling}}$. This relationship allows for the independent variation of spectral resolution, sampling and NESR.

Table 1
Characteristics of the spectral regions used in retrieval sensitivity studies. The intensity (I) is computed for every spectral region. In the UV and VIS, the Stokes parameter Q is also computed (referred to as UVQ and VISQ).

	UV/UVQ	VIS/VISQ	MIR	TIR
Wavelength	290–340 nm	560–620 nm	3035–3055 cm^{-1} 2780–2833 cm^{-1}	980–1070 cm^{-1}
Spectral Resolution (FWHM of slit function)	0.4 nm	0.4 nm	0.18 cm^{-1}	0.1 cm^{-1}
Spectral Interval (after convolution)	0.1 nm	0.1 nm	0.02775 cm^{-1}	0.06 cm^{-1}
Spectral Interval in RT calculation	0.05 nm	0.05 nm	0.0025 cm^{-1}	0.0025 cm^{-1}
SNR	3 times OMI	3 times OMI	3 times TIMS	3 times TES
Average SNR for 16 Profiles	150–3000 (I) 85–1100 (Q)	2600–3100 (I) 380–560 (Q)	86–440 (3.6 μm)	300–1250
Polarization	Yes	Yes	No	No
Scattering	Yes	Yes	Yes	No
Emission	No	No	Yes	Yes

3. Scenarios

3.1. Atmospheric profiles

The atmospheric profiles used in this simulation fall into two broad categories — 6 polluted to moderately polluted (50–110 parts per billion by volume (ppbv) O_3 in the lower troposphere), structured ozone profiles (where O_3 peaks in the boundary layer or in the layers immediately above the boundary layer) that originate from WRF-Chem regional air quality model simulations, and clean to moderately polluted ozone profiles (10–40 ppbv O_3 in the lower troposphere) that have been used in earlier TES retrieval simulations (Kulawik et al., 2006). We call the former set 'WRF-Chem profiles' and the latter set 'TES profiles'. The WRF-Chem simulation (Follette-Cook et al., personal communication) was conducted with 36-km resolution over the entire US, 12-km resolution over the eastern half of the country, and 4-km resolution over the region containing the East Coast metropolitan areas. The simulation was run for the period July 6, 2007 through July 12, 2007, which contained a severe ozone pollution episode (Yegorova et al., 2011) in the mid-Atlantic states. Profiles were selected from the 12-km output on July 9 to represent conditions ranging from strongly polluted conditions in the LMT (central New Jersey), to moderate pollution above the LMT (eastern North Carolina) resulting from long-range transport from sources to the southwest, to considerably cleaner conditions (upstate New York). Profiles were selected for three locations at two different times in the daylight hours to provide a range of solar zenith angles (SZAs). For this analysis, daytime profiles were selected, as the UV/VIS measurements are only useful during daylight hours (within some SZA constraints). The WRF-Chem model domain extended upward to 100 hPa. However, profiles from the troposphere through the stratosphere are required for this analysis. Therefore, the WRF-Chem profiles of ozone, temperature, and water vapor were extended with stratospheric profiles from the Goddard Earth Observing System – Version 5 (GEOS-5) general circulation model (Rienecker et al., 2008) to create full profiles up to 0.02 hPa. There are 47 levels (varying pressure grid in the troposphere) in these profiles, with thicker layers at higher altitudes (e.g., with 10 levels at pressure >900 hPa and 29 levels at pressure >100 hPa). The profiles from Kulawik et al. (2006) are derived from a Model for Ozone and Related Chemical Tracers-3 (MOZART-3) (Brasseur et al., 1998) run, driven with dynamic fields from the Whole Atmosphere Community Climate Model (WACCM) (Sassi et al., 2002). There are 85 levels (uniform pressure grid except for the lowest level) in these profiles (approximately 0.75 km thick except for the bottom layer which is between 1000 hPa and surface pressure). They show a range of tropopause heights and structures, and generally represent background O_3 conditions. The characteristics of the atmospheric profiles are summarized in Table 2. Note that a geostationary mission that is capable of measuring over the United States would have the potential to make measurements over the full disk, including the southern hemisphere. To study the full range of conditions, in terms of tropospheric ozone, water vapor and surface temperature, and clearly understand their impact on the measurement objectives at hand, this set of profiles was used.

The temperature and ozone profiles are illustrated in Fig. 1. Ozone profiles range from clean to polluted surface conditions and

Table 2
Key characteristics of the 16 profiles and corresponding radiative transfer calculations, including latitude, SZA, VZA, surface temperature (T_s), thermal contrast at surface (T_{contr}), total ozone column (TOZ), tropospheric ozone column (TOC), mean boundary layer ozone below 900 hPa ($O_{3,bnd}$), surface albedo in UV ($\alpha_{s,uv}$) and TIR ($\alpha_{s,ir}$), and water vapor column amount. DU stands for Dobson units. A surface albedo of 10% and 6% is assumed for VIS and MIR, respectively.

Profile Index	Lat	SZA	VZA	T_s K	T_{contr} K	TOZ DU	TOC DU	$O_{3,bnd}$ ppbv	$\alpha_{s,uv}$	$\alpha_{s,ir}$	H_2O g cm^{-2}
1	36	17	46	315	0.9	353	47	67.0	0.098	0.016	4.1
2	36	63	46	307	−5.7	351	44	61.5	0.098	0.016	4.0
3	40	22	51	312	−0.7	345	49	108.4	0.068	0.026	3.2
4	40	64	51	306	−6.3	345	47	94.3	0.068	0.026	3.1
5	44	24	54	308	−3.5	350	41	58.4	0.031	0.019	3.7
6	43	64	54	303	−8.2	348	39	57.4	0.031	0.019	3.7
7	−49	71	56	276	−3.4	393	32	31.4	0.058	0.012	0.9
8	−39	62	46	286	0.6	317	31	28.4	0.089	0.012	2.0
9	−34	58	41	284	−5.0	306	38	29.5	0.093	0.028	2.6
10	−30	54	36	299	7.5	298	41	33.1	0.077	0.021	2.0
11	−25	50	31	312	18.7	286	33	37.7	0.059	0.019	2.0
12	−20	46	28	302	6.9	264	27	19.3	0.087	0.014	3.0
13	−15	43	24	297	−1.6	264	26	17.2	0.075	0.012	3.4
14	−10	39	22	298	−0.4	266	19	17.2	0.092	0.012	3.8
15	0	33	22	298	−0.8	273	14	15.2	0.077	0.012	4.3
16	5	31	24	298	−1.2	274	12	10.3	0.092	0.012	4.8

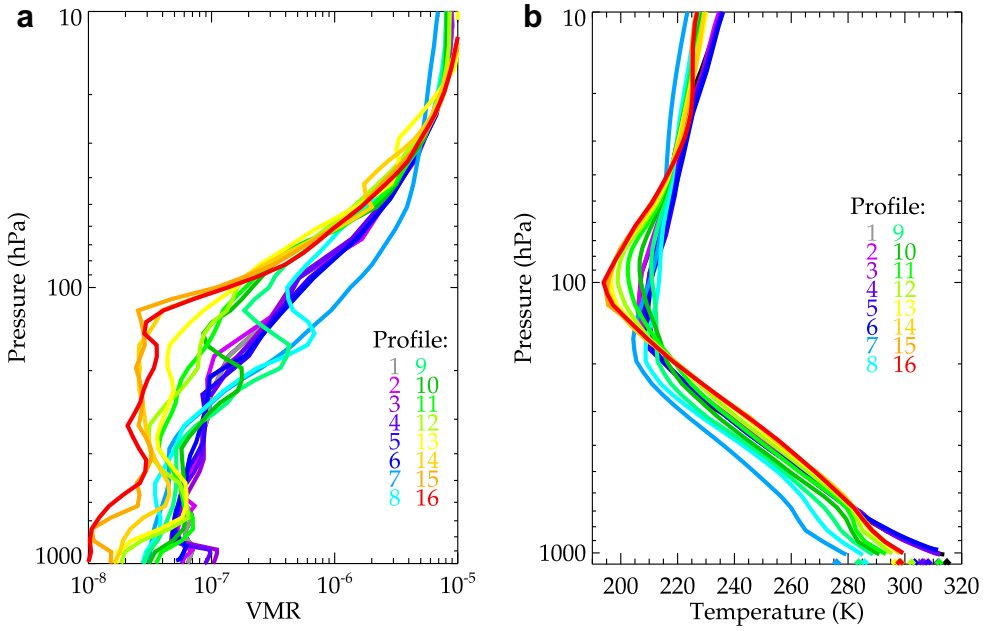

Fig. 1. The 16 ozone (left) and temperature (right) profiles used in the simulations. The surface temperature is denoted by the diamonds at the surface.

show significant variability throughout the troposphere. Profiles 1–6 (WRF-Chem profiles) have fairly similar values with variability near the surface, and profiles 7–16 (TES profiles) show more variability throughout the troposphere. A wide range of atmospheric temperatures and surface temperatures are also seen with profiles 1–6 showing fairly similar atmospheric temperatures and a varying surface temperature, and profiles 7–16 showing large variability in both the atmospheric and surface temperatures.

3.2. Surface albedo databases

In the UV, the surface albedos were interpolated from the TEMIS database (Koelemeijer et al., 2003; also on the web at http://www.temis.nl/data/ler.html). The database contains monthly minimum Lambert-equivalent reflectivity values for 1° longitude × 1° latitude grid cells at eleven 1-nm wide wavelength bins centered at 335.0, 380.0, 416.0, 440.0, 463.0, 494.5, 555.0, 610.0, 670.0, 758.0 and 772.0 nm.

In the VIS, the surface albedo was assumed to have a constant value of 0.1. For the MIR, a value of 0.06 was assumed for the albedo. Future sensitivity studies are envisaged to use a wavelength-dependent albedo in the VIS retrieval window and, for wavelengths below 500 nm, to consider the more recent OMI-derived surface albedo climatology (Kleipool et al., 2008).

The TIR emissivities are taken from the ASTER spectral library (Baldridge et al., 2009; also on the web at http://speclib.jpl.nasa.gov/) using mixes of "Ocean", "Asphalt", "Grass", "Deciduous" and "Conifer" emissivities on a 10 cm^{-1} grid, with values ranging between 0.964 and 0.989 in the spectral range used.

3.3. Solar and viewing geometry

For all of the profiles, the location and times (1 pm local time for the TES profiles, 1 pm and 5 pm local time for the WRF-Chem profiles) were used to calculate the solar viewing geometry, assuming a geostationary satellite at 95 W. The NOAA solar position calculator was used to verify the solar zenith and solar azimuth calculations (http://www.srrb.noaa.gov/highlights/sunrise/azel.html).

4. Radiative transfer model: VLIDORT

The calculations in this paper were performed using the linearized vector RT model VLIDORT (Spurr, 2006) for the numerical computation of the Stokes vector in a multiply-scattering multilayer medium. This is a plane-parallel scattering code that uses the discrete ordinate method to approximate multiple scatter integral source terms in the RT equation. VLIDORT uses the pseudo-spherical approximation for the treatment of incoming solar beam attenuation in a curved atmosphere; in addition, the model will make a precise single scatter calculation for both incoming solar and outgoing line-of-sight beams in a spherical-shell atmosphere. Stokes vector output may be generated at any level in the atmosphere and for any angular distribution, using the source function integration technique. The model can handle coupled thermal/surface emission and multiple scattering scenarios, and there is a provision for dealing with bidirectional reflecting surfaces as well as the usual Lambertian surface assumption.

The VLIDORT model is also fully linearized: simultaneously with the polarized radiance field, it will deliver analytic Jacobians with respect to any atmospheric and/or surface properties. This linearization facility is very useful for the generation of ozone and surface albedo weighting functions in the present work. VLIDORT has been validated against Rayleigh (Coulson et al., 1960) and aerosol benchmark results (Siewert, 2000). In this paper, VLIDORT was set to calculate three Stokes components (I, Q and U); circular polarization in the Earth's atmosphere was neglected.

In order to verify the new calculations in the MIR for VLIDORT, we have performed an intercomparison of radiance terms from VLIDORT and the National Center for Atmospheric Research (NCAR) GENLN Spectral Mapper (GSM) code. The NCAR GSM code is based on the GENLN line-by-line RT algorithm (Edwards, 1992), which has been compared extensively to other line-by-line codes and has been used as the basis of the fast RT processor used for CO retrievals from the Measurements of Pollution in the Troposphere (MOPITT) instrument (Edwards et al., 1999). Assuming the same atmosphere (profile 1), SZA (17°), satellite zenith angle (0°) and surface albedo (0.015), we compared monochromatic radiance terms at 2826.5 cm^{-1}, a frequency with minimal gas absorption. Radiance terms for

the thermal emission from the earth and atmosphere (attenuated by the atmosphere) and solar (transmitted, reflected at the earth's surface and attenuated by the atmosphere) were evaluated separately. The total radiance agrees to within 1% (result not shown here), which was acceptable for this comparison since we did not attempt to use the same definition for atmospheric layers or starting surface pressure (NCAR GSM set the surface to 1000 hPa, while VLIDORT used 1013 hPa, as specified in the input atmosphere).

Note that radiances in the MIR spectral region contain contributions from both solar scattering and terrestrial emission components. Hence, agreement there is a very good validation of VLIDORT. In any case, we performed similar comparisons between VLIDORT calculations and those from the NCAR GSM code in the TIR and obtained excellent agreement (better than 1%, with the same caveats as for the MIR).

5. Inverse model

In this section, we describe the method used to characterize the sensitivity of the retrievals to ozone concentration profiles, using the simulated radiances and Jacobians. Due to varying pressure grid and different number of layers (cf. Section 3.1) between the WRF-Chem and TES profiles, we perform retrievals of the logarithm of partial ozone column in each layer on the original altitude grid on which radiances and weighting functions are calculated, i.e., the retrieval grid varies from profile to profile.

5.1. Optimal estimation

Optimal estimation, with the assumption of moderate linearity, allows the estimation of retrieval errors and sensitivities. Input values are needed for radiance sensitivity to perturbations in retrieved quantities (Jacobians), radiance uncertainty (NESR), constraint matrix, atmospheric variability ($\mathbf{S}_a$), the *a priori* state ($\mathbf{x}_a$), and the true state ($\mathbf{x}$).

The linear estimate of the retrieved state ($\hat{\mathbf{x}}$) for a particular retrieval setup is:

$$\hat{\mathbf{x}} = \mathbf{x}_a + \mathbf{A}(\mathbf{x} - \mathbf{x}_a) + \mathbf{G}\mathbf{e} \tag{3}$$

where $\mathbf{A}$ is the averaging kernel, $\mathbf{G}$ is the gain matrix, and $\mathbf{e}$ is the radiance error (Rodgers, 2000). The linear estimate is a good approximation of the non-linear retrieval; Kulawik et al. (2006, 2008) found that differences between the linear estimate and non-linear retrievals for ozone in the TIR are much less than the predicted errors. Taking the covariance of the difference between the retrieved and true states, noting that the covariance of $(\mathbf{x}-\mathbf{x}_a)$ is the *a priori* covariance, $\mathbf{S}_a$, and that the covariance of the radiance error $\mathbf{e}$ is the radiance error covariance, $\mathbf{S}_m$, the estimated total retrieval error covariance, $\mathbf{S}_{\text{tot}}$, is:

$$\mathbf{S}_{\text{tot}} = (\mathbf{I} - \mathbf{A})\mathbf{S}_a(\mathbf{I} - \mathbf{A})^T + \mathbf{G}\mathbf{S}_m\mathbf{G}^T \tag{4}$$

where T stands for the transpose of the matrix and $\mathbf{I}$ is the identity matrix. The first term on the right hand side of Equation (4) is the smoothing error contribution and the second term is the random-noise error contribution. The square root of the diagonal elements of $\mathbf{S}_{\text{tot}}$, $\mathbf{S}_a$, and $\mathbf{S}_m$, are called the total retrieval error or solution error, smoothing error, and random-noise error or precision, respectively.

The retrieval sensitivity is characterized by the averaging kernel (AK), $\mathbf{A}$, the ith row of which describes how the retrieved profile in a particular layer, $\hat{\mathbf{x}}_i$, is affected by changes in the true profile, $\mathbf{x}$, in all layers. The diagonal elements of $\mathbf{A}$, known as the degrees of freedom for signal, describe the number of useful independent pieces of information available at each layer from the measurements. The trace of $\mathbf{A}$ is the total DFS for the retrieval. Similarly, the DFS for a particular altitude range (e.g., lower troposphere) can also be derived from $\mathbf{A}$ by summing up the diagonal elements of $\mathbf{A}$ for this altitude range. DFS provides an easy way of quantifying the retrieval sensitivity or information content.

5.2. Constraint matrix

To constrain the retrievals, we use climatological monthly and zonal mean ozone profiles and their standard deviations (McPeters et al., 2007) as *a priori*. This climatology is derived from a combination of ozonesonde, Stratospheric Aerosol and Gas Experiment (SAGE) and MLS data. It provides ozone mixing ratios and their standard deviations from 0 to 60 km (in pressure altitude $Z^* = -16 \times \log(P/1013)$, where P is pressure in hPa) at 1 km intervals for each month and each 10° latitude band. The cumulative columns of the climatological *a priori* and *a priori* standard deviations at the appropriate month and latitude are mapped to the retrieval grid (in logarithm of pressure) to derive *a priori* ozone and the diagonal values of the *a priori* covariance matrix so that the total column is conserved during the mapping. A correlation length of 6 km is used to construct the off-diagonal terms of the *a priori* covariance matrix $\mathbf{S}_a$. The correlation length is based on GOME retrievals (Liu et al., 2005), which has been optimized by comparing retrievals with ozonesonde observations. The correlation length has little effect on the DFS in each layer and mainly affects the retrieval errors. It should be noted that the correlation length is identical for all spectral combinations and thus will not affect the conclusions.

In addition to ozone, the state vector includes water vapor profiles (except for UV-only where there is no absorption) and surface albedo/emissivity in each spectral region. *A priori* errors of 20% and 5% are assumed for water vapor and surface albedo/emissivity respectively. Further, the *a priori* errors for non-ozone parameters are assumed to be uncorrelated with each other and with those for ozone.

6. Results

We have calculated radiances and Jacobians in all the spectral regions for the 16 cloud and aerosol free atmospheric profiles. Measurement noise is calculated according to the noise models described in Section 2.2. The *a priori* and the *a priori* covariance matrix are constructed according to Section 5.2 based on the given month and latitude corresponding to the profile. For each profile, we use the optimal estimation method to calculate averaging kernels and retrieval errors (including both random-noise errors and smoothing errors) and perform linear retrievals for all possible spectral combinations (a total of 63 combinations including individual spectral regions). From the averaging kernels, we also calculate the DFS below several key pressure levels, including top of the atmosphere, 200 hPa (surrogate for tropopause), 800 hPa (upper boundary of LMT) and 900 hPa. These DFS values can be used to summarize the retrieval sensitivities to identify the spectral combinations that might potentially meet the GEO-CAPE scientific requirements.

Table 3 lists the average DFS values for individual spectral regions and some selected spectral combinations, which include at least the UV spectral region as described in the NRC's notional GEO-CAPE mission design. For comparison, we also list the average DFS values for existing OMI and TES instruments using their own instrument characteristics. OMI and TES have low DFS in the LMT but TES has more sensitivity in the free troposphere. It is clear from the UV-only and TIR-only results in Table 3 that increasing SNR by a factor of 3 over OMI and TES, respectively, contributes to a significant increase in the total DFS. However, the increase in DFS in the

Table 3
Average total DFS and DFS at pressure levels greater than 200 hPa, 800 hPa, and 900 hPa for selected spectral combinations. For comparison, the DFS using OMI and TES characteristics are shown in the first two rows, respectively.

	Total	>200 hPa	>800 hPa	>900 hPa
OMI	4.68	1.02	0.16	0.06
TES	4.83	1.52	0.17	0.05
UV	5.89	1.39	0.26	0.12
UVQ	4.64	0.76	0.05	0.01
VIS	1.69	0.79	0.34	0.19
VISQ	1.02	0.16	0.01	0.00
MIR	1.28	0.30	0.05	0.02
TIR	6.41	1.96	0.27	0.09
UV + UVQ	6.54	1.63	0.32	0.16
UV + VIS	6.22	1.71	0.48	0.28
UV + MIR	6.01	1.42	0.26	0.12
UV + TIR	8.76	2.45	0.57	0.32
UV + VIS + UVQ	6.79	1.87	0.50	0.29
UV + VIS + TIR	8.90	2.56	0.65	0.38
UV + VIS + TIR + UVQ	9.12	2.63	0.68	0.41
UV + VIS + TIR + UVQ + VISQ + MIR	9.25	2.70	0.71	0.42

LMT is very small. This implies that the limitations of using only UV or TIR to measure lowermost tropospheric ozone cannot be overcome by improving the SNR alone. Among the spectral regions, VIS and TIR have the highest sensitivity to lowermost tropospheric and free tropospheric ozone, respectively. The MIR spectral region has low sensitivity to ozone throughout the atmosphere. Although additional VIS measurements only slightly increase the total DFS compared to the UV-only scenario, the sensitivity to the LMT is significantly enhanced; the DFS below 800 hPa almost doubles. The combination of UV and TIR can significantly improve the total DFS as well as the DFS in the LMT due to complementary vertical information throughout the atmosphere, consistent with the studies of Worden et al. (2007) and Landgraf and Hasekamp (2007). When UV is combined with more than one spectral region we find that the combination of UV, VIS and TIR provides further enhancement in sensitivity to lowermost tropospheric ozone relative to UV + TIR or UV + VIS. From all the spectral combinations, we find that the combinations of UV + VIS, UV + TIR, and UV + VIS + TIR approach or meet the GEO-CAPE measurement requirements for ozone (two degrees of freedom in the troposphere with sensitivity in the LMT) given our test set and assumptions. While the DFS and sensitivity in the LMT are important figures of merit, it is also important to consider that measurements based on the UV and VIS regions can only be made during daylight hours, whereas TIR measurements could be made at all times. One could imagine an instrument that measures all spectral regions during the day and just the TIR at night. Measurements at night may be useful in constraining model analysis even if they are only primarily sensitive to the free troposphere. The importance (or lack thereof) of nighttime measurements needs to be demonstrated with an OSSE.

Fig. 2 shows the mean and standard deviation of the DFS from the surface up to 800 (Fig. 2a) or 900 hPa (Fig. 2), averaged over the 16 atmospheric profiles. Again, VIS and TIR can be seen to add significant value to UV, with UV + TIR providing the best average results for two spectral regions and UV + VIS + TIR performing best among combinations of three spectral regions. The variability of the DFS for different profiles is around 50%, so it cannot be unequivocally established as to which combination is the best without further modeling studies or a more complete set of representative states.

Figs. 3 and 4 show examples of averaging kernels for six selected spectral combinations (UV, VIS, TIR, UV + VIS, UV + TIR, UV + VIS + TIR). Figs. 3 and 4 represent, respectively, good (profile 3) and bad (profile 14) scenarios in terms of sensitivity of the spectral regions to lowermost tropospheric ozone. For better

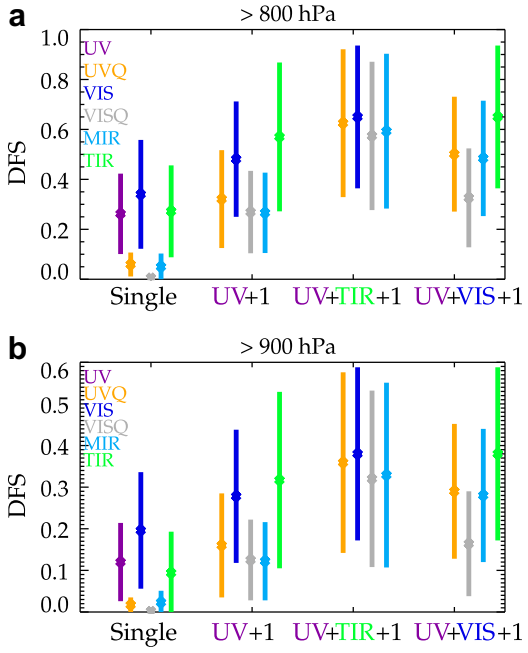

Fig. 2. Mean and standard deviation of the DFS from the surface up to 800 hPa (top), and the surface up to 900 hPa (bottom) using different spectral combinations. Results are shown for: individual spectral regions, the UV plus one additional spectral region, UV + TIR plus one additional spectral region, and UV + VIS plus one additional spectral region.

visualization of the averaging kernels, we have performed the following normalization, for the retrieved ozone in layer i corresponding to a perturbation in layer j:

$$A^{*}_{ij} = A_{ij}/\Delta z_i \quad (5)$$

The division by layer thickness Δz_i normalizes the averaging kernel to 1 km layers (Deeter et al., 2007), which is necessary because we use a variable altitude grid (varying from 20 m to 5.8 km) in the calculation and retrieval.

For the good sensitivity scenario (Fig. 3), there is an enhanced layer of ozone (108.4 ppbv) in the LMT and a high surface temperature (312 K). In the UV (Fig. 3a), the averaging kernels show a moderate peak in the lower troposphere around 890 hPa; they are generally broad in the free troposphere. The VIS averaging kernels (Fig. 3b) show a distinct peak almost at the surface, but with limited information (factor of three smaller than UV) above the LMT. The TIR averaging kernels (Fig. 3c) also show a moderate peak around 890 hPa but with stronger sensitivity (narrower peaks) from the mid troposphere to the lower stratosphere. The averaging kernel (normalized by layer thickness) shows sensitivity lower in the troposphere than usually seen for the TIR due to a combination of high thermal contrast (12 K) between 900 hPa and the surface and enhanced ozone in the lower troposphere. A shifting of sensitivity to lower altitudes in the troposphere is also seen in actual TES data with similar thermal contrast and profile characteristics. Since the averaging kernel has a finer gradation in pressure than is usual near the surface (10 layers between the surface and 900 hPa) the local peak in the Jacobian density at 890 hPa shows up in the normalized averaging kernel, whereas with the TES grid this peak would be smoothed out within the larger layer.

The combination of UV and VIS (Fig. 3d) gives a significant improvement in sensitivity to lowermost tropospheric and surface ozone compared to the UV-only scenario, but provides little improvement in the free troposphere. The combination of UV and

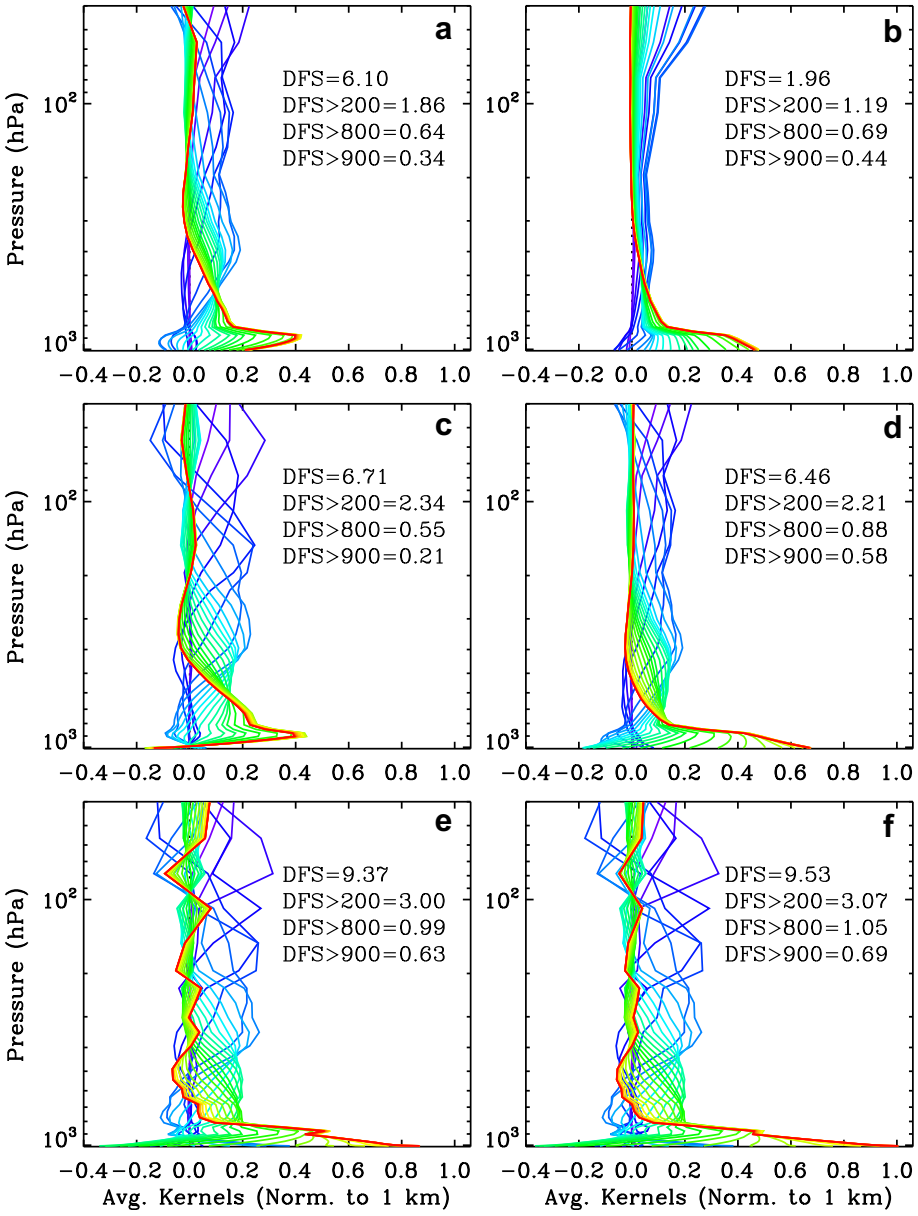

Fig. 3. Averaging kernels for selected individual and combined spectral regions for profile 3 (good sensitivity scenario). (a) UV, (b) VIS, (c) TIR, (d) UV + VIS, (e) UV + TIR, (f) UV + VIS + TIR. The averaging kernels have been normalized to 1 km layers to account for the variable altitude grid. The different colors indicate the altitude where the rows of the averaging kernels are specified, varying from purple at the top of the atmosphere to red at the surface.

TIR (Fig. 3e) also improves the sensitivity in the LMT compared to the UV-only scenario; in contrast with the UV + VIS combination, however, the UV + TIR combination also improves the sensitivity in the upper troposphere and even the stratosphere (not shown, but can be seen from the increase in the total DFS) due to more complementary vertical sensitivity than between UV and VIS. The UV + VIS + TIR combination (Fig. 3f) further improves the sensitivity in the LMT (the DFS is nearly 1 close to the surface).

For the bad sensitivity scenario (Fig. 4), there is a low amount of ozone (17 ppbv) in the LMT and a low surface temperature (298 K). In this case, UV, VIS and TIR all have limited sensitivity to lowermost tropospheric ozone. The UV averaging kernels (Fig. 4a) show a broad peak around 600 hPa. The VIS averaging kernels (Fig. 4b) show a small peak near the surface with almost no information in the free troposphere. The TIR averaging kernels (Fig. 4c) show two broad peaks in the troposphere (600 hPa and 300 hPa). The combination of VIS with UV (Fig. 4d) almost doubles the sensitivity to lowermost tropospheric ozone compared to the UV-only scenario. The combination of UV with TIR (Fig. 4e) significantly improves the sensitivity in the LMT and the upper troposphere compared to the UV-only scenario. The further addition of VIS to UV + TIR (Fig. 4f) only slightly enhances the sensitivity in the LMT.

Fig. 5a shows the DFS profiles (i.e., diagonal elements of the averaging kernels) for the six spectral combinations averaged over the 16 profiles. For UV, the average DFS does not vary much with altitude except for below 900 hPa, where it decreases with altitude because of strong Rayleigh scattering close to the surface. The DFS profile for VIS shows enhanced sensitivity in the LMT, but is much smaller than that for UV in the free troposphere. The TIR DFS profile is similar to the UV profile except that the values are larger in the free troposphere and smaller closer to the surface. The UV + VIS

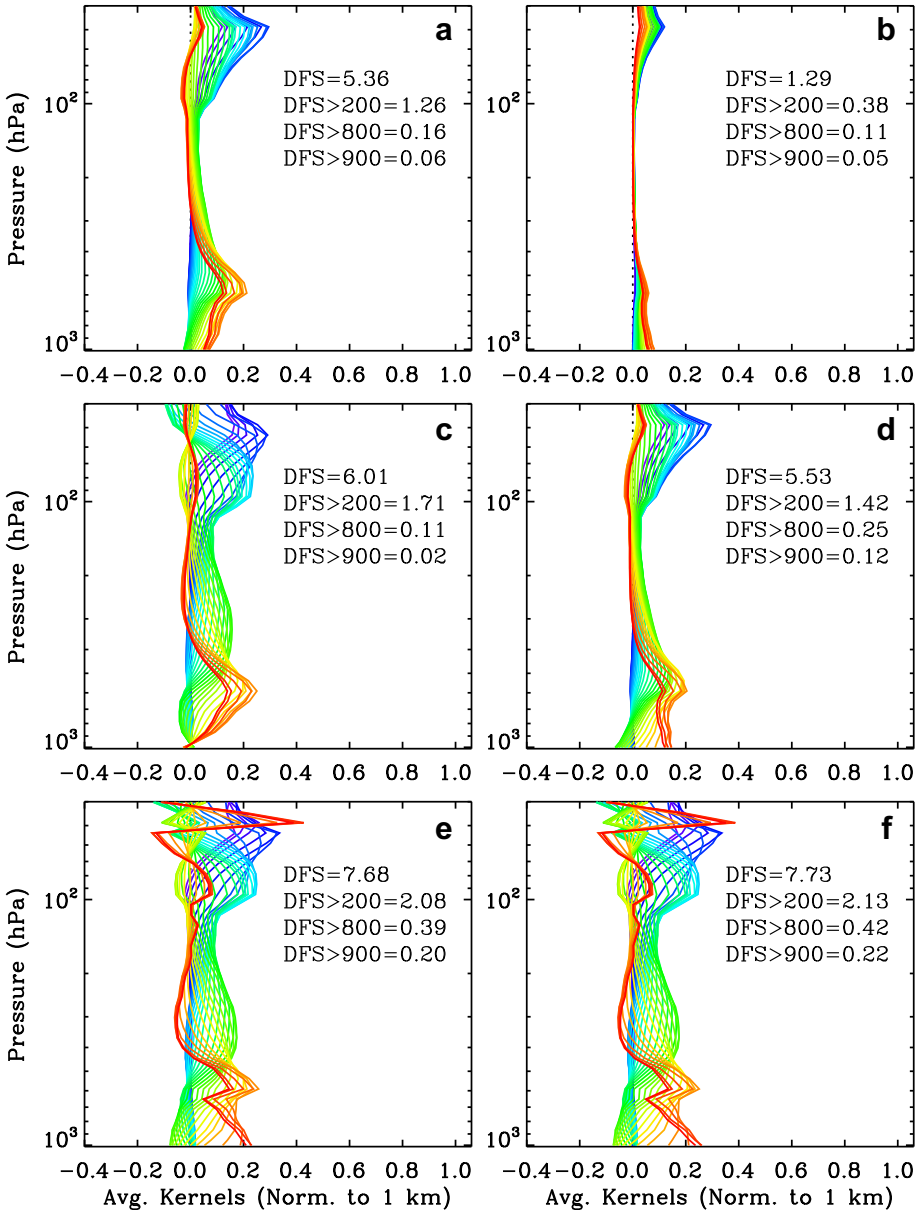

Fig. 4. Same as Fig. 3 but for profile 14 (bad sensitivity scenario).

combination mainly improves the sensitivity in the LMT relative to UV alone. The combination of TIR with UV significantly improves the sensitivity in the LMT and also improves the sensitivity in the upper troposphere. Fig. 5b shows the retrieval errors for the six spectral combinations averaged over the 16 profiles. The addition of VIS or TIR measurements to UV measurements will reduce errors in the LMT by 3–5% compared to the UV-only scenario. The addition of TIR measurements also reduces the errors in the 200–300 hPa range by ~6% compared to the UV-only scenario.

Since the retrievals cannot resolve the fine scale vertical structures, we show in Fig. 6 the retrieved ozone partial columns for four altitude ranges: surface–800 hPa, 800–500 hPa, 500–200 hPa, and surface–200 hPa, representing the LMT, mid troposphere, upper troposphere and the entire troposphere, respectively. The retrieved mean tropospheric ozone using only UV measurements agrees very well with the true values, suggesting that UV retrievals are sensitive to ozone in the troposphere, but lack the vertical sensitivity to resolve the fine scale ozone features. VIS retrievals capture the lowermost tropospheric ozone better than UV retrievals but significantly overestimate the ozone above. Compared to UV retrievals, TIR retrievals are worse in the LMT, but better in the mid and upper troposphere. The UV + VIS combination significantly improves lowermost tropospheric retrievals compared to UV alone but performs slightly worse than UV retrievals in the upper troposphere. The combination of TIR with UV resolves the vertical structures of ozone better than UV + VIS retrievals. It not only significantly improves lowermost tropospheric retrievals, like the UV + VIS scenario, but also significantly improves the retrievals in the mid and upper troposphere. The addition of VIS to UV + TIR further improves retrievals throughout the troposphere. The retrieval results are consistent with those from the DFS analysis. Supplementary figure S2 shows simulated retrievals for all pressure levels. This figure shows the capability of spectral combinations to resolve features in the true profile. Of particular interest is the capability of UV, VIS and TIR combinations to resolve the surface pollution event seen in profiles 3 and 4.

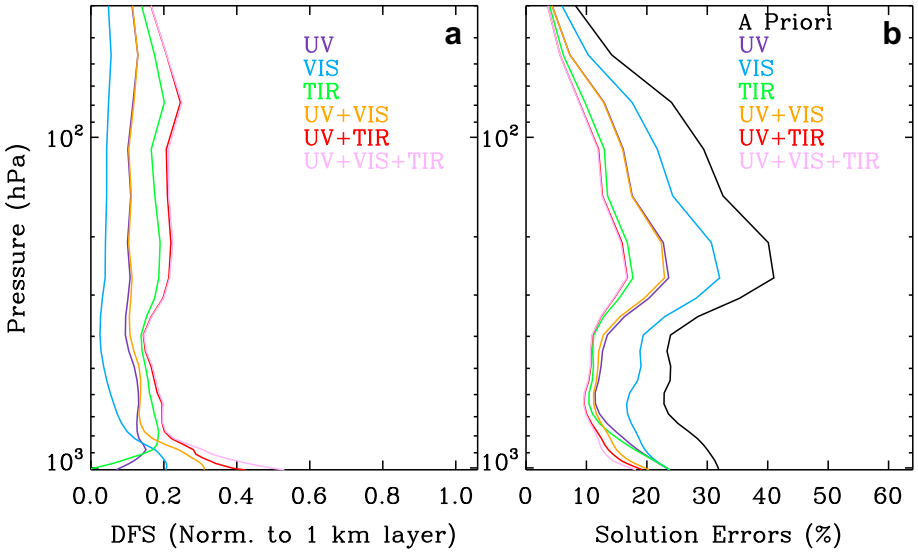

Fig. 5. (a) Profiles of DFS in each layer (normalized to 1 km layers), (b) Solution errors. Results shown are averaged over the 16 atmospheric profiles.

7. Discussion

7.1. Effects of spectral resolution, sampling interval and SNR

To investigate how retrieval sensitivity varies with spectral resolution, sampling interval, and SNR, we repeat the above analysis for the six selected spectral combinations by perturbing the parameters listed in Table 1 one at a time. The retrieval sensitivities in terms of mean DFS for four altitude ranges are summarized in Table 4. Note that when spectral resolution is changed the sampling interval remains the same so that the SNR remains constant. It is evident that the DFS values do not vary much with the spectral resolution, especially in the UV and VIS due to the broad ozone absorption structures. TIR retrievals are more sensitive to the spectral resolution, but the effects are still small. Changing the spectral resolution from 0.05 cm^{-1} to 0.4 cm^{-1} only decreases the lowermost tropospheric DFS from 0.29 to 0.21. Compared to the spectral resolution, the SNR has a much larger impact on the retrieval sensitivity for all the spectral combinations; the relative change in DFS values is especially large in the LMT. The lowermost tropospheric DFS increases by 65–105% when the SNR is increased by a factor of 4. In all the above scenarios, the main conclusions about the need for combining VIS and/or TIR with UV to improve tropospheric and lowermost tropospheric retrieval sensitivity remain true.

Since changes in sampling interval hardly affect the results when the spectral resolution and SNR per unit wavelength are fixed, Table 5 does not show results for perturbations to the sampling interval. However, although these theoretical results are insensitive to the sampling interval, having adequate spectral samples per instrument slit function is important for real satellite retrievals in the UV/VIS to reduce spectral interpolation errors resulting from relative radiance/irradiance wavelength shifts (Chance et al., 2005).

7.2. Effects of polarization and surface model

The use of degree of linear polarization measurements in the UV (i.e., $-Q/I$) has been proposed to improve tropospheric ozone retrievals from satellite (Hasekamp and Landgraf, 2002; Hasekamp et al., 2002; Jiang et al., 2004) and ground-based (Jiang et al., 1997, 2004; Guo et al., 2007) measurements. We examined the sensitivity of polarization measurements to atmospheric ozone retrievals. The average DFS values over the 16 profiles are listed in Table 5. The DFS for degree of linear polarization measurements (UVPOL) is much smaller than that for radiance (UV) or Stokes parameter Q (UVQ) measurements due to information cancellation when taking the ratio Q/I. The addition of polarization measurements to radiance measurements only slightly improves sensitivity to lowermost tropospheric ozone. These results seem to contradict previous studies (Hasekamp and Landgraf, 2002; Hasekamp et al., 2002; Jiang et al., 2004), which show that polarization measurements are mainly sensitive to ozone in the troposphere and adding polarization measurements even at a few wavelengths to radiance measurements can significantly enhance sensitivity to ozone in the lower troposphere. This is because the sensitivity of polarization measurements to tropospheric ozone depends strongly on the viewing geometry. Liu et al. (2009) studied the enhancement in tropospheric ozone retrieval sensitivity by adding polarization measurements to radiance measurements in the UV for a standard US atmosphere and a wide range of viewing geometries (with both SZA and viewing zenith angle (VZA) ranging from 0° to 85°). It was found that the polarization contribution normally increases with large SZA or VZA. Most of the enhancements due to polarization measurements peak in the mid troposphere.

In the above calculations, we assumed the surface to be Lambertian. This is a good assumption for land. However, over the ocean, the surface is highly non-Lambertian and polarizing. To account for this, we performed calculations in the UV (including polarization) over the ocean using the Cox and Munk polarized bidirectional reflection model (Cox and Munk, 1954; Mishchenko and Travis, 1997). The wind speed was assumed to be 5 m s^{-1}. The calculations were performed for regular GEO-CAPE viewing geometry and for sun glint geometry (SZA = VZA, azimuth angle = 0). It is evident from Table 5 that when only radiance measurements are used, there is some enhancement in ozone retrieval sensitivity in the LMT compared to a Lambertian surface. However, when polarization is considered, the DFS in the LMT almost doubles. This sensitivity test suggests that polarization measurements may provide additional information when the surface is polarizing.

7.3. Spectroscopy and calibration consistency

One important source of systematic error that will need to be addressed when combining TIR and UV spectral measurements is the current discrepancy between UV and TIR spectroscopic

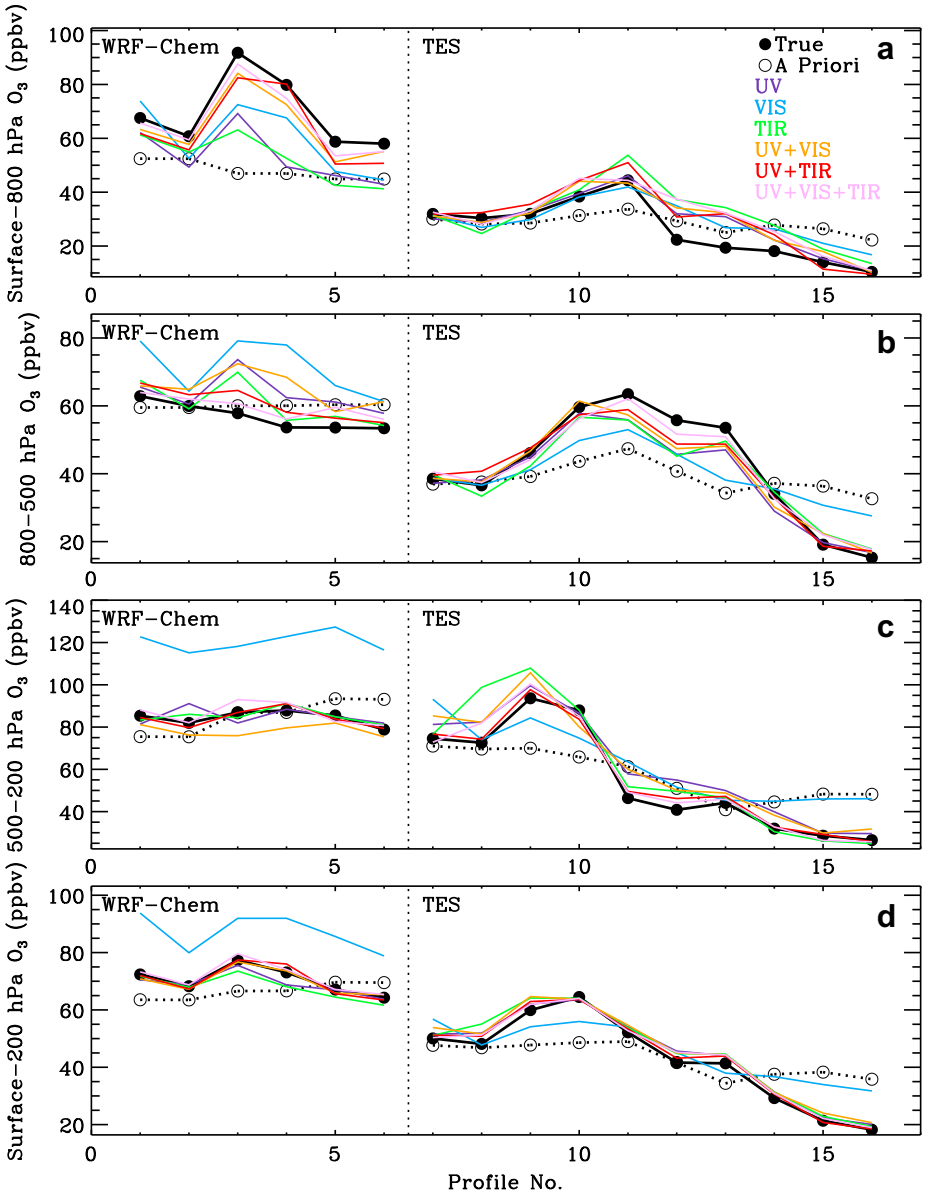

Fig. 6. Mean ozone mixing ratio averaged between (a) surface–800 hPa, (b) 800–500 hPa, (c) 500–200 hPa, (d) surface–200 hPa *vs*. atmospheric profile number for true, *a priori*, and retrievals for the six selected spectral combinations from Fig. 3. The atmospheric profiles are arranged in the same order as in Table 2. Profiles 1–6 correspond to the WRF-Chem profiles and profiles 7–16 correspond to the TES profiles.

parameters. This discrepancy has been quantified in a laboratory intercomparison (Picquet-Varrault et al., 2005), with TIR to UV differences of 5.5%. Intercomparisons of ground-based total ozone column measurements using Brewer and Fourier Transform Infrared (FTIR) instruments (Schneider et al., 2008) show a systematic difference of 4.5% for FTIR – Brewer total columns. Validation results for satellite ozone profiles and columns from TIR observations also show a consistent high bias compared to ozonesondes and UV/VIS measurements (such as GOME-2 and OMI) (see, e.g., Boynard et al., 2009; Nassar et al., 2008; Osterman et al., 2008) Future versions of the HITRAN spectroscopic database (Rothman et al., 2005) should address this discrepancy; however, if it is not completely mitigated, other corrections to the forward model or retrieval may be necessary, such as a retrieved or fixed line strength correction factor. The spectral discrepancy in the UV versus the TIR is observed in comparisons of TES and OMI ozone estimates, where a high bias (~15%) is seen by TES relative to OMI. If this relative bias is not accounted for, it results in 'jackknifing' of the joint retrieval (Kulawik et al., 2007). We did not include the effects of inconsistent spectroscopy in the analysis for this paper (cf. Section 2.1).

Another important challenge for combining multi-spectral regions is the radiometric calibration consistency among different spectral regions. This has been a critical issue even for ozone profile retrievals using two channels from current satellite measurements. Because of the large dynamic range of signal (several orders of magnitude) in the Hartley-Huggins bands, current UV measurements are measured in two channels (split ~310 nm), which have different spatial resolution and calibration characteristics. Normally, empirical corrections based on the comparison between simulations with known ozone profile measurements and observations are necessary to combine both channels (Krijger et al., 2005; Liu et al., 2007; van der et al., 2002). Preliminary attempts to linearly combine OMI and TES retrievals lead to unrealistic

Table 4
Comparison of DFS for different spectral resolutions and SNRs. The spectral resolution and SNR are specified relative to those used in Table 1.

Trade-off runs		Total	>200 hPa	>800 hPa	>900 hPa
Twice better spectral resolution	UV	5.93	1.41	0.26	0.11
	VIS	1.69	0.79	0.34	0.19
	TIR	6.95	2.06	0.29	0.10
	UV + VIS	6.26	1.72	0.48	0.27
	UV + TIR	9.17	2.53	0.58	0.32
	UV + VIS + TIR	9.30	2.63	0.66	0.38
Twice worse spectral resolution	UV	5.79	1.36	0.25	0.11
	VIS	1.69	0.79	0.34	0.19
	TIR	5.93	1.85	0.24	0.08
	UV + VIS	6.13	1.68	0.47	0.27
	UV + TIR	8.38	2.36	0.54	0.29
	UV + VIS + TIR	8.54	2.48	0.63	0.37
Four times worse spectral resolution	UV	5.55	1.27	0.24	0.10
	VIS	1.69	0.79	0.34	0.19
	TIR	5.55	1.72	0.21	0.06
	UV + VIS	5.91	1.61	0.47	0.27
	UV + TIR	8.08	2.27	0.51	0.28
	UV + VIS + TIR	8.26	2.41	0.61	0.35
Half SNR	UV	5.12	1.16	0.19	0.08
	VIS	1.38	0.54	0.22	0.12
	TIR	5.37	1.67	0.20	0.06
	UV + VIS	5.35	1.37	0.34	0.19
	UV + TIR	7.49	2.08	0.43	0.23
	UV + VIS + TIR	7.58	2.15	0.49	0.27
Double SNR	UV	6.66	1.65	0.33	0.15
	VIS	2.04	1.06	0.45	0.25
	TIR	7.65	2.28	0.37	0.15
	UV + VIS	7.12	2.05	0.62	0.37
	UV + TIR	10.14	2.83	0.70	0.41
	UV + VIS + TIR	10.33	2.97	0.81	0.49

oscillation features in the combined profiles due to a combination of calibration and spectroscopic inconsistencies. So it is important to ensure calibration consistency between various spectral regions especially for improving tropospheric and lowermost tropospheric ozone retrievals.

The Chappuis band has long been used to make precise ozone measurements with solar occultation (see, e.g., McCormick et al., 1989) or limb scattering techniques (see, e.g., McPeters et al., 2000). However, it has not been used to improve UV ozone retrievals from current satellite measurements (e.g., GOME, SCIAMACHY, GOME-2) in the nadir viewing geometry, where surface reflection can significantly contribute to the measured radiances. The weak and broad ozone absorption in this band implies that the retrievals are very sensitive to radiometric calibration errors and require a good knowledge of the spectral variation of surface albedo. In current satellite measurements, the Chappuis band is measured in two different channels/detectors split near the peak of the Chappuis band. Data quality normally degrades at the channel edge and there are offsets between the two channels. Accurate radiometric calibration is necessary to utilize current satellite measurements. As for the spectral variation of the surface albedo, if it is linearly dependent on wavelength, sensitivity studies show that it is possible to estimate the spectral dependence directly from measurements. *A priori* knowledge might be needed for more complex spectral structures in surface albedo. During follow-on GEO-CAPE activities, we plan to use existing satellite or aircraft measurements to examine if the spectral variation of surface albedo is problematic to retrievals for various surface conditions.

Table 5
Comparison of DFS using UV or UVQ for three different surface models, including Lambertian surface used in above analysis, ocean bidirectional polarization distribution function (BPDF) with the same viewing geometry, and ocean BPDF with sun glint viewing geometry (VZA = SZA, relative azimuth angle = zero). UVPOL denotes the degree of linear polarization ($-Q/I$) in the UV.

Surface Model		Total	>200 hPa	>800 hPa	>900 hPa
Lambertian	UV	5.89	1.39	0.26	0.12
	UVQ	4.64	0.76	0.05	0.01
	UVPOL	2.26	0.99	0.18	0.08
	UV + UVQ	6.54	1.63	0.32	0.16
Ocean BPDF (same viewing geometry)	UV	5.92	1.42	0.27	0.13
	UVQ	4.79	0.90	0.12	0.05
	UV + UVQ	6.62	1.77	0.42	0.23
Ocean BPDF (sun glint)	UV	6.18	1.54	0.37	0.19
	UVQ	5.13	1.08	0.27	0.14
	UV + UVQ	6.93	1.91	0.52	0.30

7.4. Aerosol/cloud properties

In the above analysis, we have not considered the effects of clouds and aerosols on retrieval sensitivity as well as their interferences to ozone retrievals if their properties are not accurately known. This work is in progress and will be the topic of a subsequent paper. However, a short discussion is in order here. The TIR channels should help minimize the influence of small aerosol particles because their extinction goes down in a linear to quadratic fashion with wavelength. Further, even if there is some extinction due to these particles in the TIR, they behave like Rayleigh scatterers at these wavelengths, and hence the net effect is simply a perturbation to the Rayleigh optical depth. On the other hand, the UV/VIS channels should help constrain cirrus and water clouds, and large non-absorbing aerosol particles because their extinction does not change much between the different spectral regions, as opposed to the strongly wavelength-dependent nature of ozone absorption. Further, the use of polarization (especially in the UV/VIS channels) should provide further information on the microphysical properties of aerosols and clouds (see, e.g., Mishchenko and Travis, 1997), which can in turn be used to improve ozone retrievals.

8. Conclusions

In this paper, we have begun the characterization, through the simulation of 16 profiles, of the sensitivity of multi-spectral retrieval to lowermost tropospheric ozone, which is a requirement of the GEO-CAPE mission. Spectral regions, spectral resolution, and noise characteristics were specified using best guess estimates of how existing spaceborne and ground-based instruments could be improved. An optimal estimation framework was employed to perform linearized retrievals to assess the retrieval errors and sensitivity.

For cloud- and aerosol free simulations, a pragmatic starting point, we find that no spectral band alone appears to have the needed sensitivity specified by the GEO-CAPE science requirements. If VIS wavelengths are added to UV measurements, the lowermost tropospheric ozone sensitivity is enhanced, but the change in the total DFS is small. The lowermost tropospheric and total DFS are both improved when UV is combined with TIR. The MIR spectral region does not add significant information for ozone at any vertical level. In order to meet the GEO-CAPE science requirements, viz., to measure ozone with two degrees of freedom in the troposphere with sensitivity in the lowest 2 km, an innovative approach, such as a multi-spectral retrieval, is required. In addition, a multi-spectral approach that includes TIR could make measurements at night, whereas use of solely the UV and VIS bands would be limited to daylight measurements only.

Recently, Zoogman et al. (2011) conducted an OSSE to evaluate the ability of geostationary measurements in different spectral regions to constrain surface ozone concentrations through data

assimilation. Their results are consistent with our analyses; VIS measurements are effective in reducing analysis errors when the thermal contrast is small while TIR measurements help when the thermal contrast is large. Although their study is limited by the use of fixed AKs for cloud/aerosol free conditions and fixed viewing geometry, it provides an example of the way in which case-specific sensitivity studies of the type presented here may be generalized to a full examination of the impact of a candidate observation, or set of observations, in meeting a prescribed measurement requirement.

This is the start of a program of work and, as such, the results should be regarded as encouraging but preliminary. Further work is needed to add increasing sophistication to the cloud and aerosol free simulations presented here. Studies are in progress to update the described framework to include gas and temperature interferents, a range of cloud and aerosol scenarios, and more realistic surface properties, and to optimize the spectral ranges of some of the spectral regions (e.g., VIS). These calculations will in turn allow for an evaluation of how multi-spectral retrieval sensitivity to lowermost tropospheric ozone will change over all the observational conditions expected for GEO-CAPE. This will be expressed through variable averaging kernel matrices responding to changes in environmental conditions, and these will be used by future OSSEs of the type conducted by Zoogman et al. (2011). It is expected that these experiments will provide a means for quantitatively evaluating the expected performance, of candidate multi-spectral instrumentation, and observing strategies with improved retrieval vertical information relevant to air quality forecasts, in meeting the measurement requirements of GEO-CAPE.

To conclude, spectroscopic measurements of ozone in different wavelength bands, corresponding to different molecular transitions, provide concentration information that samples the atmospheric profile differently. Combined measurements of carefully selected combinations of wavelength bands, e.g., UV + VIS or UV + TIR, can provide improved knowledge of the concentration in the troposphere, including its lowermost part (enabling better characterization of air quality), over that from measurements in a single wavelength region.

Acknowledgments

A portion of this work was carried out at the Jet Propulsion Laboratory, California Institute of Technology. Funding for this effort was provided by the Earth Science Division of the NASA Science Mission Directorate. X.L. was funded by the Aura OMI project. The National Center for Atmospheric Research is sponsored by the National Science Foundation. The authors would like to thank the two anonymous reviewers for their insightful suggestions that undoubtedly improved the quality of the paper.

Appendix. Supplementary data

Supplementary data associated with this article can be found, in the online version, at doi:10.1016/j.atmosenv.2011.09.014.

References

Akimoto, H., 2003. Global air quality and pollution. Science 302 (5651), 1,716–1,719,. doi:10.1126/science.1092666.

Akimoto, H., et al., 2008. Planning a geostationary atmospheric observation satellite. Commission on the Atmospheric Observation Satellite of the Japan Society of Atmospheric Chemistry (JSAC), Atmospheric Composition Research Program, Frontier Research Center for Global Change, Japan Agency for Marine-Earth Science and Technology (JAMSTEC), 3173–25 Showa-machi, Kanazawa-ku, Yokohama City, Kanagawa, 236-0001.

Akimoto, H., Kasai, Y., Kita, K., Irie, H., Sagi, K., Hayashida, S., 2009. Geostationary Atmospheric Observation Satellite Plan in Japan. Eos, Transactions, American Geophysical Union 90(52), Fall Meeting Supplement, Abstract A51M-03.

Atlas, R., 1997. Atmospheric observations and experiments to assess their usefulness in data assimilation. Journal of the Meteorological Society of Japan 75, 111–130.

Aumann, H.H., et al., 2003. AIRS/AMSU/HSB on the Aqua mission: design, science objectives, data products, and processing systems. IEEE Transactions on Geoscience and Remote Sensing 41 (2), 253–264. doi:10.1109/TGRS.2002.808356.

Baldridge, A.M., Hook, S.J., Grove, C.I., Rivera, G., 2009. The ASTER spectral library version 2.0. Remote Sensing of Environment 113 (4), 711–715. doi:10.1016/j.rse.2008.11.007.

Beer, R., 1992. Remote Sensing by Fourier Transform Spectrometry. John Wiley & Sons, New York.

Beer, R., 2006. TES on the Aura mission: scientific objectives, measurements, and analysis overview. IEEE Transactions on Geoscience and Remote Sensing 44 (5), 1,102–1,105. doi:10.1109/TGRS.2005.863716.

Boubel, R.W., Fox, D.L., Turner, B., Stern, A.C., 1994. Fundamentals of Air Pollution, third ed. Academic Press, San Diego.

Bovensmann, H., et al., 1999. SCIAMACHY: mission objectives and measurement modes. Journal of the Atmospheric Sciences 56 (2), 127–150. doi:10.1175/1520-0469(1999)056<0127:SMOAMM>2.0.CO;2.

Bowman, K.W., Steck, T., Worden, H.M., Worden, J., Clough, S., Rodgers, C., 2002. Capturing time and vertical variability of tropospheric ozone: a study using TES nadir retrievals. Journal of Geophysical Research 107 (D23), 4723,. doi:10.1029/2002JD002150.

Boynard, A., et al., 2009. Measurements of total and tropospheric ozone from IASI: comparison with correlative satellite, ground-based and ozonesonde observations. Atmospheric Chemistry and Physics 9 (16), 6,255–6,271,. doi:10.5194/acp-9-6255-2009.

Brasseur, G.P., et al., 1998. MOZART, a global chemical transport model for ozone and related chemical tracers. 1. Model description. Journal of Geophysical Research 103 (D21), 28,265–28,289,. doi:10.1029/98JD02397.

Brion, J., Chakir, A., Charbonnier, J., Daumont, D., Parisse, C., Malicet, J., 1998. Absorption spectra measurements for the ozone molecule in the 350–830 nm region. Journal of Atmosheric Chemistry 30 (2), 291–299. doi:10.1023/A:1006036924364.

Brion, J., Chakir, A., Daumont, D., Malicet, J., Parisse, C., 1993. High-resolution laboratory absorption cross section of O_3. Temperature effect. Chemical Physics Letters 213 (5–6), 610–612. doi:10.1016/0009-2614(93)89169-I.

Burrows, J.P., et al., 1993. Rep. ESA SP-1151. In: Guyenne, T.D., Readings, C. (Eds.), Global Ozone Monitoring Experiment Interim Science Report. ESA Publications Division, ESTEC, Noordwijk, The Netherlands.

Burrows, J.P., et al., 2004. The geostationary tropospheric pollution explorer (GeoTROPE) missions: objects requirements and mission concept. Advances in Space Research 34 (4), 682–687. doi:10.1016/j.asr.2003.08.067.

CEOS, 2011. A Geostationary Satellite Constellation for Observing Global Air Quality: An International Path Forward (Draft version 4.0), CEOS Atmospheric Composition Constellation. Available online at. http://www.ceos.org/index.php?option=com_content&view=category&layout=blog&id=54&Itemid=95, 41 pp.

Chance, K.V., Burrows, J.P., Perner, D., Schneider, W., 1997. Satellite measurements of atmospheric ozone profiles, including tropospheric ozone, from ultraviolet/visible measurements in the nadir geometry: a potential method to retrieve tropospheric ozone. Journal of Quantitative Spectroscopy and Radiative Transfer 57 (4), 467–476. doi:10.1016/S0022-4073(96)00157-4.

Chance, K.V., Burrows, J.P., Schneider, W., 1991. Retrieval and molecule sensitivity studies for the global ozone monitoring experiment and the SCanning imaging absorption spectroMeter for atmospheric CHartographY. In: Proceedings of SPIE, Remote Sensing of Atmospheric Chemistry, pp. 151–165. doi:10.1117/12.46657. 1491.

Chance, K., Kurosu, T.P., Sioris, C.E., 2005. Undersampling correction for array detector-based satellite spectrometers. Applied Optics 44 (7), 1,296–1,304. doi:10.1364/AO.44.001296.

Claeyman, M., et al., 2011. A thermal infrared instrument onboard a geostationary platform for CO and O_3 measurements in the lowermost troposphere: observing System Simulation Experiments. Atmospheric Measurement Techniques 4 (8), 1,637–1,661. doi:10.5194/amt-4-1637-2011.

Clerbaux, C., et al., 2009. Monitoring of atmospheric composition using the thermal infrared IASI/MetOp sounder. Atmospheric Chemistry and Physics 9 (16), 6,041–6,054. doi:10.5194/acp-9-6041-2009.

Coulson, K.L., Dave, J.V., Sekera, Z., 1960. Tables Related to Radiation Emerging from a Planetary Atmosphere with Rayleigh Scattering. University of California Press, Berkeley, California.

Cox, C., Munk, W., 1954. Statistics of the sea surface derived from sun glitter. Journal of Marine Research 13 (2), 198–227. doi:10.1364/JOSA.44.000838.

Daumont, M., Brion, J., Charbonnier, J., Malicet, J., 1992. Ozone UV spectroscopy. I: absorption cross-sections at room temperature. Journal of Atmospheric Chemistry 15 (2), 145–155. doi:10.1007/BF00053756.

Deeter, M.N., Edwards, D.P., Gille, J.C., Drummond, J.R., 2007. Sensitivity of MOPITT observations to carbon monoxide in the lower troposphere. Journal of Geophysical Research 112, D24306. doi:10.1029/2007JD008929.

Dufour, G., Eremenko, M., Orphal, J., Flaud, J.-M., 2010. IASI observations of seasonal and day-to-day variations of tropospheric ozone over three highly populated areas of China: Beijing, Shanghai, and Hong Kong. Atmospheric Chemistry and Physics 10, 3,787–3,801. doi:10.5194/acp-10-3787-2010.

Edwards, D.P., 1992. GENLN2: a General Line-by-line Atmospheric Transmittance and Radiance Model. Version 3.0: Description and Users Guide, Rep. NCAR/TN-367–STR. National Center for Atmospheric Research, Boulder, Colorado.

Edwards, D.P., Halvorson, C.M., Gille, J.C., 1999. Radiative transfer modeling for the EOS Terra satellite measurement of pollution in the troposphere (MOPITT)

instrument. Journal of Geophysical Research 104 (D14), 16,755–16,775. doi:10.1029/1999JD900167.
Edwards, D.P., Arellano Jr., A.F., Deeter, M.N., 2009. A satellite observation system simulation experiment for carbon monoxide in the lowermost troposphere. Journal of Geophysical Research 114, D14304. doi:10.1029/2008JD011375.
Eremenko, M., et al., 2008. Tropospheric ozone distributions over Europe during the heat wave in July 2007 observed from infrared nadir spectra recorded by IASI. Geophysical Research Letters 35, L18805. doi:10.1029/2008GL034803.
European Space Agency, 1995. Rep. ESA SP-1182. In: Bednarz, F. (Ed.), The GOME Users Manual. ESA Publications Division, ESTEC, Noordwijk, The Netherlands.
Guo, X., et al., 2007. Retrieval of ozone profile from ground-based measurements with polarization: a synthetic study. Journal of Quantitative Spectroscopy and Radiative Transfer 103 (1), 175–192. doi:10.1016/j.jqsrt.2006.05.008.
Hasekamp, O.P., Landgraf, J., 2002. Tropospheric ozone information from satellite-based polarization measurements. Journal of Geophysical Research 107 (D17), 4326. doi:10.1029/2001JD001346.
Hasekamp, O.P., Landgraf, J., van Oss, R., 2002. The need of polarization modeling for ozone profile retrieval from backscattered sunlight. Journal of Geophysical Research 107 (D23), 4692. doi:10.1029/2002JD002387.
IPCC, 2007. In: Core Writing Team, Pachauri, R.K., Reisinger, A. (Eds.), Climate Change 2007: Synthesis Report. Contribution of Working Groups I, II and III to the Fourth Assessment Report of the Intergovernmental Panel on Climate Change, p. 104. Geneva, Switzerland.
Jiang, Y., Yung, Y.L., Sander, S.P., 1997. Detection of tropospheric ozone by remote sensing from the ground. Journal of Quantitative Spectroscopy and Radiative Transfer 57 (6), 811–818. doi:10.1016/S0022-4073(96)00145-8.
Jiang, Y., Yung, Y.L., Sander, S.P., Travis, L.D., 2004. Modeling of atmospheric radiative transfer with polarization and its application to the remote sensing of tropospheric ozone. Journal of Quantitative Spectroscopy and Radiative Transfer 84 (2), 169–179. doi:10.1016/S0022-4073(03)00140-7.
Jourdain, L., et al., 2007. Tropospheric vertical distribution of tropical Atlantic ozone observed by TES during the northern African biomass burning season. Geophysical Research Letters 34, L04810. doi:10.1029/2006GL028284.
Kalnay, E., 2003. Atmospheric Modeling, Data Assimilation and Predictability. Cambridge University Press, Cambridge.
Kim, J., et al., 2009. Monitoring Air Quality from Geostationary Orbit in Asia-Pacific Region by MP-GEOSAT. Eos, Transactions, American Geophysical Union 90(52), Fall Meeting Supplement, Abstract A52C-01.
Kleipool, Q.I., Dobber, M.R., de Haan, J.F., Levelt, P.F., 2008. Earth surface reflectance climatology from 3 years of OMI data. Journal of Geophysical Research 113 (D18), D18308. doi:10.1029/2008JD010290.
Koelemeijer, R.B.A., de Haan, J.F., Stammes, P., 2003. A database of spectral surface reflectivity in the range 335–772 nm derived from 5.5 years of GOME observations. Journal of Geophysical Research 108 (D2). doi:10.1029/2002JD002429.
Krijger, J.M., Aben, I., Landgraf, J., 2005. CHEOPS-GOME: WP2.1: Study of Instrument Degradation. Rep. SRON-EOS/RP/05–018. ESA Publications Division, ESTEC, Noordwijk, The Netherlands.
Kulawik, S.S., Bowman, K.W., Luo, M., Rodgers, C.D., Jourdain, L., 2008. Impact of nonlinearity on changing the a priori of trace gas profile estimates from the Tropospheric Emission Spectrometer (TES). Atmospheric Chemistry and Physics 8 (12), 3,081–3,092. doi:10.5194/acp-8-3081-2008.
Kulawik, S.S., et al., 2006. TES atmospheric profile retrieval characterization: an orbit of simulated observations. IEEE Transactions on Geoscience and Remote Sensing 44 (5), 1,324–1,333. doi:10.1109/TGRS.2006.871207.
Kulawik, S.S., et al., 2007. Optimally Combining Ozone from Tropospheric Emission Spectrometer (TES) and Ozone Monitoring Instrument (OMI) Data. Eos, Transactions, American Geophysical Union 88(52), Fall Meeting Supplement, Abstract A33C-1403.
Kumer, J.B., Roche, A.E., Rairden, R.L., De Souza-Machado, S.G., Chatfield, R.B., 2009. Assessing the Information Content of the Tropospheric Infrared Mapping Spectrometers (TIMS) GEO-CAPE Instrument Concept when Applied for Several Infrared Ozone Bands. Eos, Transactions, American Geophysical Union 90(52), Fall Meeting Supplement, Abstract A53A-0242.
Kumer, J.B., Roche, A.E., Rairden, R.L., Jamieson, T.H., Mergenthaler, J.L., Chatfield, R.B., 2008. GEO-CAPE Application, Demonstrated for CO by the IIP Tropospheric Infrared Mapping Spectrometers (TIMS), and Scaled to an Expanded Application that Adds the 9.6, 3.3 and 3.6 μm bands for Multi-layer Tropospheric Ozone and for HCHO. Eos, Transactions, American Geophysical Union 89(52), Fall Meeting Supplement, Abstract IN24A-03.
Landgraf, J., Hasekamp, O.P., 2007. Retrieval of tropospheric ozone: the synergistic use of thermal infrared emission and ultraviolet reflectivity measurements from space. Journal of Geophysical Research 112, D08310. doi:10.1029/2006JD008097.
Langen, J., 2007. GMES Sentinels 4 and 5 Mission Requirements Document EOP-SMA/1507/JL-dr.
Lee, S., et al., 2010. Plan of Korean geostationary environment satellite over Asia-Pacific region. Geophysical Research Abstracts 12 Abstract EGU2010-7595-1.
Levelt, P.F., et al., 2006. The ozone monitoring instrument. IEEE Transactions on Geoscience and Remote Sensing 44 (5), 1,093–1,101. doi:10.1109/TGRS.2006.872333.
Liu, X., Bhartia, P.K., Chance, K., 2009. Monitoring of Tropospheric Ozone from Backscattered Ultraviolet Measurements on Geostationary Platforms. Eos, Transactions, American Geophysical Union 90(52), Fall Meeting Supplement, Abstract A53A-0243.
Liu, X., Bhartia, P.K., Chance, K., Froidevaux, L., Spurr, R.J.D., Kurosu, T.P., 2010a. Validation of Ozone Monitoring Instrument (OMI) ozone profiles and stratospheric ozone columns with Microwave Limb Sounder (MLS) measurements. Atmospheric Chemistry and Physics 10 (5), 2,539–2,549. doi:10.5194/acp-10-2539-2010.
Liu, X., Bhartia, P.K., Chance, K., Spurr, R.J.D., Kurosu, T.P., 2010b. Ozone profile retrievals from the ozone monitoring instrument. Atmospheric Chemistry and Physics 10 (5), 2,521–2,537. doi:10.5194/acp-10-2521-2010.
Liu, X., Chance, K., Kurosu, T.P., 2007. Improved ozone profile retrievals from GOME data with degradation correction in reflectance. Atmospheric Chemistry and Physics 7, 1575–1583.
Liu, X., et al., 2005. Ozone profile and tropospheric ozone retrievals from the global ozone monitoring experiment: algorithm description and validation. Journal of Geophysical Research 110, D20307. doi:10.1029/2005JD006240.
Liu, X., et al., 2006. First directly retrieved global distribution of tropospheric column ozone from GOME: comparison with the GEOS-CHEM model. Journal of Geophysical Research 111, D02308. doi:10.1029/2005JD006564.
Malicet, J., Daumont, D., Charbonnier, J., Parisse, C., Chakir, A., Brion, J., 1995. Ozone UV spectroscopy. II. Absorption cross-sections and temperature dependence. Journal of Atmospheric Chemistry 21 (3), 263–273. doi:10.1007/BF00696758.
Martin, R.V., 2008. Satellite remote sensing of surface air quality. Atmospheric Environment 42 (34), 7,823–7,843. doi:10.1016/j.atmosenv.2008.07.018.
Masutani, M., et al., 2010. Observing system simulation experiments at the National Centers for environmental prediction. Journal of Geophysical Research 115, D07101. doi:10.1029/2009JD012528.
McCormick, M.P., Zawodny, J.M., Veiga, R.E., Larsen, J.C., Wang, P.H., 1989. An overview of SAGE I And II ozone measurements. Planetary and Space Science 37 (12), 1,567–1,586. doi:10.1016/0032-0633(89)90146-3.
McPeters, R.D., Janz, S.J., Hilsenrath, E., Brown, T.L., Flittner, D.E., Heath, D.F., 2000. The retrieval of O_3 profiles from limb scatter measurements: results from the Shuttle ozone limb Sounding experiment. Geophysical Research Letters 27 (17), 2,597–2,600. doi:10.1029/1999GL011342.
McPeters, R.D., Labow, G.J., Logan, J.A., 2007. Ozone climatological profiles for satellite retrieval algorithms. Journal of Geophysical Research 112 (D5), D05308. doi:10.1029/2005JD006823.
Mishchenko, M.I., Travis, L.D., 1997. Satellite retrieval of aerosol properties over the ocean using polarization as well as intensity of reflected sunlight. Journal of Geophysical Research 102 (D14), 16,989–17,013. doi:10.1029/96JD02425.
Nassar, R., et al., 2008. Validation of Tropospheric Emission Spectrometer (TES) nadir ozone profiles using ozonesonde measurements. Journal of Geophysical Research 113 (D15), D15S17. doi:10.1029/2007JD008819.
National Research Council, 2007. Earth Science and Applications from Space: National Imperatives for the Next Decade and beyond, Committee on Earth Science and Applications from Space: A Community Assessment and Strategy for the Future. National Academies Press, Washington, D. C.
OMI Algorithm Theoretical Basis Document, 2002. In: Bhartia, P.K. (Ed.), OMI Ozone Products, vol II. NASA Goddard Space Flight Center, Greenbelt, Maryland. Rep. ATBD-OMI-02.
Osterman, G., et al., 2008. Validation of Tropospheric Emission Spectrometer (TES) measurements of the total, stratospheric and tropospheric column abundance of ozone. Journal of Geophysical Research 113 (D15), D15S16. doi:10.1029/2007JD008801.
Picquet-Varrault, B., Orphal, J., Doussin, J.-F., Carlier, P., Flaud, J.-M., 2005. Laboratory intercomparison of the ozone absorption coefficients in the mid-infrared (10 μm) and ultraviolet (300–350 nm) spectral regions. Journal of Physical Chemistry A 109 (6), 1,008–1,014. doi:10.1021/jp0405411.
Rienecker, M.M., et al., 2008. The GEOS-5 Data Assimilation System—Documentation of Versions 5.0.1, 5.1.0, and 5.2.0. In: Technical Report Series on Global Modeling and Data Assimilation, NASA/TM–2008–104606, vol. 27. Global Modeling and Assimilation Office, NASA Goddard Space Flight Center, Greenbelt, Maryland.
Rodgers, C.D., 2000. Inverse Methods for Atmospheric Sounding: Theory and Practice. World Scientific Publishing, Singapore.
Rothman, L.S., et al., 2005. The HITRAN 2004 molecular spectroscopic database. Journal of Quantitative Spectroscopy and Radiative Transfer 96 (2), 139–204. doi:10.1016/j.jqsrt.2004.10.008.
Rothman, L.S., et al., 2009. The HITRAN 2008 molecular spectroscopic database. Journal of Quantitative Spectroscopy and Radiative Transfer 110 (9–10), 533–572. doi:10.1016/j.jqsrt.2009.02.013.
Sassi, F., Garcia, R.R., Boville, B.A., Liu, H., 2002. On temperature inversions and the mesospheric surf zone. Journal of Geophysical Research 107 (D19), 4380. doi:10.1029/2001JD001525.
Schneider, M., Redondas, A., Hase, F., Guirado, C., Blumenstock, T., Cuevas, E., 2008. Comparison of ground-based Brewer and FTIR total column O_3 monitoring techniques. Atmospheric Chemistry and Physics 8 (18), 5,535–5,550. doi:10.5194/acp-8-5535-2008.
Seinfeld, J.H., Pandis, S.N., 2006. Atmospheric Chemistry and Physics: From Air Pollution to Climate Change, second ed. John Wiley and Sons, Inc., New York.
Siewert, C.E., 2000. A discrete-ordinates solution for radiative-transfer models that include polarization effects. Journal of Quantitative Spectroscopy and Radiative Transfer 64 (3), 227–254. doi:10.1016/S0022-4073(99)00006-0.
Spurr, R.J.D., 2006. VLIDORT: a linearized pseudo-spherical vector discrete ordinate radiative transfer code for forward model and retrieval studies in multilayer multiple scattering media. Journal of Quantitative Spectroscopy and Radiative Transfer 102 (2), 316–342. doi:10.1016/j.jqsrt.2006.05.005.
Stuhlmann, R., et al., 2005. Plans for EUMETSAT's third generation meteosat geostationary satellite programme. Advances in Space Research 36 (5), 975–981. doi:10.1016/j.asr.2005.03.091.

Timmermans, R.M., et al., 2009. The added value of a proposed satellite imager for ground level particulate matter analyses and forecasts. IEEE Journal of Selected Topics in Applied Earth Observations and Remote Sensing 2 (4), 271–283. doi:10.1109/JSTARS.2009.2034613.

van der, A.R.J., van Oss, R.F., Piters, A.J.M., Fortuin, J.P.F., Meijer, Y.J., Kelder, H.M., 2002. Ozone profile retrieval from recalibrated global ozone monitoring experiment data. Journal of Geophysical Research 107 (D15), 4,239. doi:10.1029/2001JD000696.

Worden, H., et al., 2006. . TES level 1 algorithms: interferogram processing, geolocation, radiometric, and spectral calibration. IEEE Transactions on Geoscience and Remote Sensing 44 (5), 1,288–1,296. doi:10.1109/TGRS.2005.863717.

Worden, J., et al., 2004. Predicted errors of Tropospheric Emission Spectrometer nadir retrievals from spectral window selection. Journal of Geophysical Research 109 (D9), D09308. doi:10.1029/2004JD004522.

Worden, J., et al., 2007. Improved tropospheric ozone profile retrievals using OMI and TES radiances. Geophysical Research Letters 34, L01809. doi:10.1029/2006GL027806.

Yegorova, E.A., Allen, D.J., Loughner, C.P., Pickering, K.E., Dickerson, R.R., 2011, Characterization of an eastern U.S. severe air pollution episode using WRF/Chem. Journal of Geophysical Research, 116., D17306, doi:10.1029/2010JD015054.

Ziemke, J.R., et al., 2006. Tropospheric ozone determined from Aura OMI and MLS: evaluation of measurements and comparison with the global modeling Initiative's chemical transport model. Journal of Geophysical Research 111, D19303. doi:10.1029/2006JD007089.

Zoogman, P., et al., 2011. Ozone air quality measurement requirements for a geostationary satellite mission. Atmospheric Environment. doi:10.1016/j.atmosenv.2011.05.058.